Degradation Capacity Spatial-Temporal Embedding RUL Prediction Framework for Lithium-ion Batteries

Laijin Luo, Yu Wang, *IEEE Senior Member*, Yang Li, *IEEE Senior Member*, and Qiushi Cui, *IEEE Member*

***Abstract*—Accurately predicting the remaining useful life (RUL) of lithium-ion batteries is crucial to ensure the safe and reliable operation of the energy storage and power supply systems. However, RUL prediction is significantly affected by the challenges posed by multi-dimensional nonlinearity. Embedding spatial-temporal variables helps reveal nonlinear relationships, making the degradation capacity spatial-temporal embedding an effective approach for extracting patterns and trends of battery degradation within multi-dimensional subspaces. Motivated by this, this work proposes a phase space reconstruction (PSR) approach that utilizes the C–C method combined with a convolutional neural network-bidirectional LSTM and hyperspace attention mechanism (CNN-BiLSTM-HAM) to address this challenge. First, the C-C method performs PSR according to time delay and embedding dimension values to transform degradation capacity data from one-dimensional time series into a multi-dimensional format. Next, the reconstructed capacity matrix is processed by the CNN to generate feature vectors that preserve the spatial structure and location information of the input data, while discarding irrelevant information. These feature vectors serve as input for training the BiLSTM. Finally, the HAM is used to allocate the weights of different feature subsets simultaneously. The proposed CNN-BiLSTM-HAM model and C–C method are validated using the NASA dataset. Experimental results demonstrate that the proposed method yields accurate RUL prediction, with the absolute error, mean absolute error, and root mean square error all being less than 2, 1.3%, and 2%, respectively.**

***Index Terms*—Lithium-ion batteries, remaining useful life, capacity spatial-temporal embedding, convolutional neural network, bidirectional long short-term memory, hyperspace attention mechanism.**

I. Introduction

THE energy storage system plays an increasingly critical role in modern energy and transportation systems, strongly supported by global energy-saving and emission-reduction policies [1],[2]. The lithium-ion battery is an environmentally friendly, high-energy, recyclable energy storage solution [3]. It has become integrated into the daily lives of consumers, powering devices like smartphones, laptops, and electric vehicles (EVs) [4],[5]. Despite their advantages, the increasing usage of lithium-ion batteries will inevitably cause performance degradation [6], which can lead to issues such as capacity loss, reduced driving range, and shortened service life [7]. Consequently, when the battery's maximum available capacity falls to the failure threshold, i.e., typically 70 to 80% of its nominal capacity [8],[9],[10], it can no longer reliably power EVs. Timely battery replacement is essential to avoid increased safety risks [11]. To accurately monitor the power, safety, and reliability of the entire energy storage system, it is crucial to design an effective approach for predicting the battery's remaining useful life (RUL), which also enables early warning of potential battery failure [12], [13].

Many researchers have conducted in-depth exploration into methods of battery RUL prediction over the past few years. There are three main categories of RUL prediction methods—model-based [14], data-driven [15], and hybrid approaches [16]—as summarized in Table I. Model-based approaches require an accurate physical degradation model that describes the complex electrochemical behaviors inside a battery. However, these approaches involve extensive parameterization and computational efforts, resulting in many challenges in implementation and application [17]. In contrast, data-driven and hybrid approaches do not demand detailed battery physical parameters, such as convolutional neural network (CNN) [18], support vector machine (SVM) [19], and long short-term memory (LSTM) [20],[21]. They only require sufficient historical operating data to obtain more accurate battery capacity predictions [22].

For example, Saxena et al. [18] predicted capacity decay curves utilizing discharging voltage data as CNN input. However, the current is sensitive to fluctuation with load variations in real working conditions, resulting in a predictive model that might fail to match the actual battery voltage behavior. In order to enhance the SVM, Swain et al. [19] built a more comprehensive battery capacity degradation model that combined the one-way analysis of variance to validate the impact of aging factors, such as temperature change and usage cycle, on battery capacity. Zraibi et al. [20] combined the advantages of CNN and LSTM to extract temporal and spatial features from discharge capacity data for battery RUL prediction. This not only provided an effective method for constructing a deep hybrid model but also demonstrated that the hybrid model is superior to a single model. Lyu et al. [21] extracted aging features from partial charging data to establish an offline SVM-based capacity estimation model. The model uses LSTM to predict aging features in real time, which are then incorporated into an offline model for RUL prediction. This approach provides novel insights for indirect RUL

This work was supported by the Fundamental Research Funds for the Central Universities of China (2023CDJYXTD-004). (Corresponding author: Yu Wang)

Laijin Luo, Yu Wang, and Qiushi Cui are with School of Electrical Engineering, Chongqing University, Chongqing, China (e-mail: 20241101048@stu.cqu.edu.cn; yu_wang@cqu.edu.cn; qcui@cqu.edu.cn).

Yang Li is with Department of Electrical Engineering, Chalmers University of Technology, 41296 Gothenburg, Sweden (e-mail: yangli@ieee.org).

prediction and health management.

Although CNN, LSTM, and SVM have achieved notable success in battery RUL prediction, they present various limitations. For example, while CNN is excellent in extracting abstract features in image processing, it is difficult to establish temporal dependencies in time series data. Meanwhile, SVM, as a commonly used supervised learning method, often relies on expert knowledge to perform reliable feature engineering. LSTM can memorize and update the input data information through the unique logic gates, but its unidirectional structure restricts the model to learning information soley from past time steps. In addition, the regeneration phenomenon during battery aging can easily cause deviations in capacity data. Therefore, using the bidirectional structure of BiLSTM to learn information from both past and future time steps offers an effective solution for improved prediction accuracy and overcoming the above challenges [22].

TABLE I
COMPARISON OF THREE RUL PREDICTION METHODS

Method	Advantages	Disadvantages
Model-based	High interpretability; low data requirements	Complex modeling and parameter identification
Data-driven	Adaptable to diverse patterns; high accuracy	High data dependency and lack of interpretability
Hybrid approaches	Combines strengths of both approaches	Increased complexity; needs data and expertise

Notably, in data-driven and hybrid approaches, data dimension is important for the effectiveness of the algorithm. Overly large data dimensions and lengths can increase model complexity and lead to overfitting on the training set, resulting in poor performance on unseen data. Small data lengths and dimensions fail to capture long-term dependencies that are important for making accurate predictions. According to Takens' theorem, choosing an appropriate time delay and embedding dimension is critical for effectively predicting nonlinear time series [18]. Therefore, determining the dimension and length of input data is a challenging but crucial task. The C–C method proposed by Kim et al., which utilizes two correlation integrals and is named after the statistical concept, can be effectively used to calculate the embedding dimension and time delay in solving non-linear time series prediction problems [19],[20]. Particularly, phase space reconstruction with the C–C method offers the advantage of better capturing the nonlinear relationships and dynamics buried in the data. This capability contributes to enhanced feature extraction, analysis, and modeling accuracy. On the other hand, the presence of the capacity regeneration phenomenon causes the nonlinear problem to exhibit varying degradation rate trends at different stages, making it difficult to capture the dynamic changes in battery capacity over time. Specifically, available capacity will recover briefly or even increase compared to the previous cycle, with an amplitude typically ranging from 0% to 5%. However, this is often followed by a faster decay in battery capacity during the subsequent cycle [21]. This capacity regeneration phenomenon can cause a failure to accurately reflect the overall trend of changes and reduce the confidence level in the predicted results.

In order to resolve the above issues, this paper proposes a novel convolutional neural network bidirectional LSTM with hyperspace attention mechanism (CNN-BiLSTM-HAM) structure as well as a capacity data phase space reconstruction (PSR) technique for reducing prediction error and improving the performance of battery health monitoring. In the PSR technique, we drop the classical strategy of using a fixed moving window for a one-dimensional time series. Instead, we perform spatio-temporal embedding by mapping one-dimensional capacity data into a high-dimensional space and determining appropriate time delay and embedding dimension values. This approach ensures that the complex nonlinear dynamics of different degradation rate stages are captured in a more comprehensive way. Meanwhile, by considering the interdependence between different degradation stages within the capacity data embedded through spatial-temporal dimensions, valuable coupling features are automatically extracted through the convolutional and pooling layers of the CNN. The BiLSTM effectively models the accurate temporal dependencies of each degradation rate stage, enhancing the reliability and accuracy of RUL prediction. To tackle the heterogeneity and complexity of degradation rates, we propose the HAM to selectively and dynamically adjust the weights of different degradation rate stages. The main contributions and novelties of this research are outlined as follows:

1) A methodology is introduced for embedding spatial-temporal degradation capacity data based on PSR with the C–C method. This proposed approach enhances data dimensionality and reconstruction, allowing the network to extract more valuable information and prepare for more effective training in subsequent steps.

2) A hybrid prediction model based on CNN-BiLSTM-HAM is constructed. In this model, CNN is employed to extract a rich feature map from the reconstructed matrix (including dimension and length of capacity data). The BiLSTM network consists of two independently and inversely processed LSTM layers, allowing it to capture information from both past and future time steps simultaneously. At the same time, each LSTM selectively forgets and stores information in the input data based on memory units and gating structures to achieve an accurate prediction of the battery regeneration part. The HAM captures underlying relationships between different time steps and allocates learnable weights to enhance the representation of significant information at each time step.

3) A framework for predicting the RUL is constructed by combining the C-C method with the CNN-BiLSTM-HAM hybrid model. This structure transforms traditional one-dimensional capacity data into a higher-dimensional space, enabling the capture of hyperspace-level dynamic degradation. This approach offers new perspectives for understanding lithium-ion battery degradation mechanisms and effectively

This article has been accepted for publication in IEEE Journal of Emerging and Selected Topics in Industrial Electronics. This is the author's version which has not been fully edited and content may change prior to final publication. Citation information: DOI 10.1109/JESTIE.2025.3561664

bridges the gap between simple models and high-dimensional degradation features.

The benefits of the proposed approach are demonstrated by comparing it with LSTM, BiLSTM, CNN-BiLSTM, CNN-BiLSTM with single-head attention (CNN-BiLSTM-SHA), and CNN-BiLSTM-HAM methods. Furthermore, the performances of these methods are validated by establishing different prediction starting points (30, 50, and 70) in the experimental analysis.

The remainder of this work is arranged as follows. Section II introduces established model methodologies and the proposed prediction frameworks, including the C-C method, CNN algorithm, BiLSTM algorithm, and HAM algorithm. Section III focuses on the experimental datasets, and four error metrics are used to analyze and discuss the predicted results of the comparison experiments. Section IV summarizes the key findings.

II. Proposed Methodology

A. Proposed RUL Prediction Framework.

The proposed framework of the RUL prediction process is presented in Fig.1, based on the C-C method and the CNN-BiLSTM-HAM hybrid model proposed in this paper. In this approach, the C-C method is used to embed spatial-temporal capacity data and determine the size of the capacity reconstruction matrix. By stacking multiple convolutional layers, the model achieves multi-level feature extraction, which contributes to better uncovering abstract features and underlying patterns. The BiLSTM effectively captures bidirectional dependencies within the data by comprehensively considering both past and future information at each time step. Finally, the HAM is introduced to process the weight assignments of different feature subsets in parallel, which enables precise forecasting of battery capacity degradation trends.

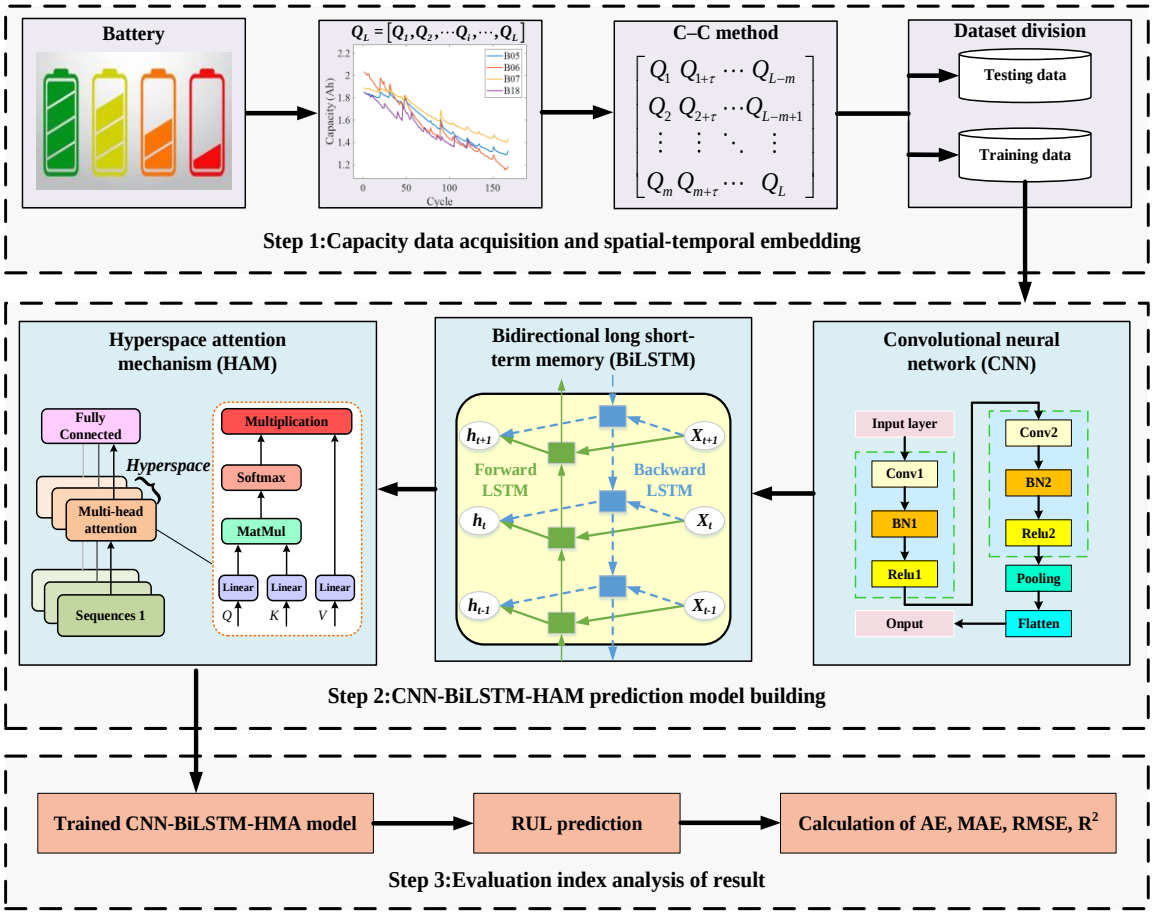

Fig. 1. Proposed RUL prediction framework based on C-C method and CNN-BiLSTM-HAM.

Specifically, the proposed prediction framework is divided into the following three steps:

Step 1: Capacity data acquisition and spatial-temporal embedding. Degradation sequence data of the battery capacity are obtained from NASA. Then the time delay and embedding dimension m are determined by the C-C method for reconstructing a capacity matrix. Different starting points of the capacity cycle are set to divide the data into training and testing sets.

Step 2: Construction of prediction model. First, the reconstructed capacity matrix is input into a CNN containing two convolutional layers (kernel size of 2×2) to extract complex features. Next, the CNN outputs are fed into the BiLSTM network that simultaneously considers bidirectional dependencies to overcome capacity regeneration phenomenon at relevant moments. Finally, the output is calculated through

weighted summation based on the hyperspace attention matrix derived from combining the multi-head attention score matrix in different sub-spaces.

Step 3: Evaluation index analysis of the result. The established CNN-BiLSTM-HAM model is trained for RUL prediction, and the predicted results are evaluated using four performance indicators.

B. Spatio-Temporal Embedding of Capacity Data With the C–C Method

The C-C method is based on two correlation integrals to calculate the time delay and the embedding dimension. It is worth mentioning that the C-C method is very suitable for time series problems in nonlinear systems [20,21]. The capacity data of the battery can be represented as a time series $Q_L = [Q_1, Q_2, \cdots Q_i, \cdots, Q_L]$. The correlation integral can be described as:

$$C(m, L, r, \tau) = \frac{2}{M(M-1)} \sum_{1 \le i}^{M} \sum_{i < j}^{M} F(r - \|Q_i - Q_j\|) \tag{1}$$

where $M = L - (m-1)\tau$ represents the number of embedded points in the m-dimensional space, L is the size of the capacity time series data, r denotes the space distance, and τ indicates the reconstructed delay. Here F represents a function: if $x \ge 0$, then $F(x) = 1$; if $x < 0$, then $F(x) = 0$.

Next, the statistic S is a characteristic function to describe nonlinearity in a time series. S can be calculated by the following partitioning averaging strategy:

$$S(m, L, r, \tau) = \frac{1}{\tau} \sum_{S=1}^{\tau} \left[C_s(m, \frac{L}{\tau}, r, \tau) - C_s^m(1, \frac{L}{\tau}, r, \tau) \right] \tag{2}$$

Assuming m and τ are fixed, as L approaches infinity, S will be constant and equal to 0 for all space distance r. Normally, the collected data is limited and likely to be correlated in practice. Thus, $S(m, L, r, \tau) \neq 0$. Further, the optimal delay τ can be either the first zero crossings of $S(m, L, r, \tau)$ or location where the minimum rate of variation of $S(m, L, r, \tau)$ with respect to r. By selecting two representative r_j, the following quantity is defined:

$$\Delta S(m, \tau) = \max\{S(m, r_j, \tau)\} - \min\{S(m, r_j, \tau)\} \tag{3}$$

where $S(m, r_j, \tau) = \lim_{L \to \infty} S(m, L, r_j, \tau)$, as these two quantities on the RHS of (3) can be considered equally important, the optimal delay problem can be transformed into finding the minimum of $\Delta S(m, \tau)$. In order to do this, we define the following variable:

$$S_{cor} = \Delta \bar{S}(\tau) + |\bar{S}(\tau)| \tag{4}$$

where $\Delta \bar{S}(\tau)$ and $\bar{S}(\tau)$ represent the average values of $\Delta S(m, \tau)$ and $S(m, r_j, \tau)$, respectively. The minimum of S_{cor} denotes the time delay window τ_w, and the first zero crossing of $\bar{S}(\tau)$ or the first local minimum of $\Delta \bar{S}(\tau)$ denotes the time delay τ_d, thereby, the embedding dimension m can be obtained by solving $\tau_w = (m-1)\tau_d$.

According to (2)-(4), the delay and embedding dimension of the reconstructed matrix can be calculated. In this paper, the embedding dimension is the length of the time window. The relationship between the original capacity time series and the reconstructed capacity matrix is shown in (5), which facilitates the understanding of the subsequent CNN feature map extraction process.

$$\begin{bmatrix} Q_1 \\ Q_2 \\ \vdots \\ Q_i \\ \vdots \\ Q_L \end{bmatrix} \rightarrow \begin{bmatrix} Q_1 & Q_{1+\tau} & \cdots & Q_{L-m} \\ Q_2 & Q_{2+\tau} & \cdots & Q_{L-m+1} \\ \vdots & \vdots & \ddots & \vdots \\ Q_m & Q_{m+\tau} & \cdots & Q_L \end{bmatrix} \tag{5}$$

C. Convolution Neural Network

As mentioned earlier, conventional RUL prediction approaches for batteries face the challenge of the relatively small amount of available data and the presence of complex nonlinear degradation [15]. However, CNN has brought new perspectives for RUL prediction with its remarkable feature extraction capability. A basic CNN usually consists of four types of layers, including the convolution layer, activation layer, pooling layer, and fully connected layer. The formula for discrete two-dimensional convolution is as follows:

$$O(i, j) = \sum_{p} \sum_{q} I(i+p, j+q) * K(p, q) \tag{6}$$

where $O(i, j)$ is the element of the ith row and jth column of the output feature map, $I(i+p, j+q)$ represents the input element of the $i+p$th row and $j+q$th column; $K(p, q)$ denotes the element of the pth row and qth column of the convolution kernel.

We designed a CNN with an eight-layer structure, consisting of two convolutional layers, two batch normalization layers, two ReLU activation layers, one pooling layer, and one flattening layer. The convolutional kernel size is selected as 2×2, which can balance computational resources while exploring more feature combinations; batch normalization layers normalize the data to approximate a Gaussian distribution, helping to accelerate training and prevent gradient vanishing or explosion.

D. Bidirectional Long Short-Term Memory

Deep learning technology, as a powerful artificial intelligence tool, is driving advancements across various fields [16]. Owing to its excellent performance in processing sequence data and forecasting tasks, LSTM has been regarded as an essential RNN. A basic LSTM cell consists of three control gates, including forgetting gate f_t, input gate i_t, and output gate o_t. Furthermore, the LSTM cell also depends on storing the long-term state C_t and short-term state h_t. The cell architecture of LSTM is shown in Fig. 2. The governing equations of each LSTM cell are given as follows:

$$f_t = \sigma(w_f[h_{t-1}, x_t] + b_f) \tag{7}$$

$$i_t = \sigma(w_i[h_{t-1}, x_t] + b_i) \tag{8}$$

$$\tilde{c}_t = \tanh(w_c[h_{t-1}, x_t] + b_c) \tag{9}$$

$$o_t = \sigma(w_o[h_{t-1}, x_t] + b_o) \tag{10}$$

$$C_t = f_t \odot C_{t-1} + i_t \odot \tilde{c}_t \tag{11}$$

$$h_t = o_t \odot \tanh(S_t) \tag{12}$$

where σ represents the sigmoid function; w and b are the corresponding weight and bias matrices of the corresponding control gate, respectively; x_t and h_{t-1} denote input at time t, and the output of the previous LSTM cell at time t-1, respectively; C_t and C_{t-1} represent cell states at time t and t-1 respectively; $\odot$ is the Hadamard product, which can be viewed as intermediate variables.

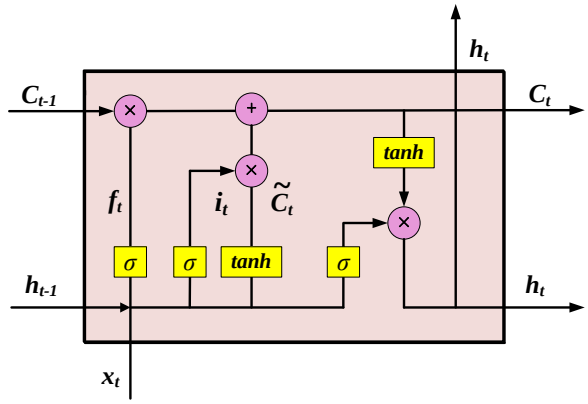

Fig. 2. Cell architecture of LSTM.

The BiLSTM network layer is composed of a forward and a backward passing information LSTM layer. The output result h_t can be calculated after obtaining the forward LSTM hidden layer state $\vec{h}_t$, and the backward LSTM hidden layer state $\overleftarrow{h}_t$, i.e.,

$$\vec{h}_t = f(x_t, \vec{h}_{t-1}) \tag{13}$$

$$\overleftarrow{h}_t = f(x_t, \overleftarrow{h}_{t-1}) \tag{14}$$

$$h_t = \vec{w}_t \vec{h}_t + \overleftarrow{w}_t \overleftarrow{h}_t + b_t \tag{15}$$

where $\vec{w}_t$ and $\overleftarrow{w}_t$ are the weight of forward and backward LSTM hidden layer, respectively; output result h_t is a linear combination of forward and backward LSTM, plus a bias b_t.

E. Hyperspace Attention Mechanism.

Conventional attention mechanism typically employs an attention weight distribution to weight the input data. The drawbacks of this strategy include the lack of parallelism and the unbalance of learning information in a single-head self-attention mechanism [17]. To address these issues, we propose the hyperspace attention mechanism (HAM), applied after the spatial-temporal embedding of capacity data and extraction of global spatial features from CNN.

Furthermore, capacity degradation is influenced by various internal and external factors, resulting in multi-phase and variable-rate patterns that are difficult to distinguish in one-dimensional data. Yet, these complex and variable degradation patterns are more effectively represented in hyperspace. Therefore, by introducing the HAM, the model can privilege vital time periods and features that significantly affect capacity evolution for improving prediction performance and adjusting dynamics between different sub-spaces. The HAM approach addresses the issue of significant multi-space hidden state loss, enhancing the model's forecasting capabilities for both short-term and long-term predictions. Denoting the time series to be processed $\boldsymbol{X} \in \boldsymbol{R}^{n \times d_x}$ and n is the dimension of input capacity data segment, the query matrix $Q = XW_Q$ and key matrix $K = XW_k$ in the same k-dimension, the value matrix $V = XW_v$ can be reconstructed in v-dimension by a linear transformation. Formally, the output of the single-head attention mechanism is acquired as follows:

$$Attention(Q, K, V) = \text{soft}\max\left(\frac{QK^T}{\sqrt{d_k}}\right)V \tag{16}$$

where T represents the transpose operation and $\sqrt{d_k}$ is a scaling factor for the dot product attention.

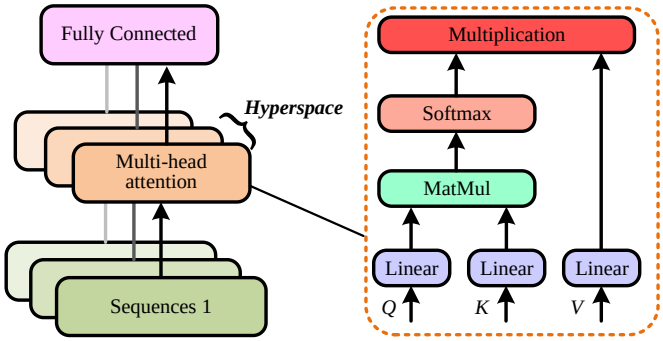

Fig. 3. Architecture of a hyperspace attention mechanism.

However, the single-head attention mechanism struggles to achieve comprehensive attention when processing data across multiple sub-spaces. In this regard, the HAM is designed to enhance the prediction process of the battery capacity variations, as illustrated in Fig. 3. Specifically, based on the C-C method, the capacity matrix is reconstructed in multiple sub-spaces, the multi-head attention is independently applied within each sub-space to calculate the dot-product attention scores. Finally, these score matrices are combined into a hyper-space attention matrix, which serves as the input to the fully connected layer. The computational process of HAM can be expressed as follows:

$$MH = Concat(head_1, \ldots, head_i, \ldots, head_h)W^o \tag{17}$$

$$HAM = \sigma(MH * W_{space} + b_{space}) \tag{18}$$

where *Concat* is the matrix concatenation operation, $head_i = Attention(Q_i, K_i, V_i)$, W^o represents the weight matrix, h indicates the number of attention heads, $i \in \{1, 2, \ldots, h\}$; W_{space} and b_{space} denote the weight and bias matrix in different sub-spaces, respectively, σ represents the sigmoid function.

III. Case Study

A. Dataset Description and Normalization

In this work, the lithium-ion battery dataset provided by the National Aeronautics and Space Administration (NASA) was utilized to demonstrate the proposed RUL prediction framework. Among them, the four 18650 cells with a nominal capacity of 2 Ah are numbered B0005, B0006, B0007, and B0018, respectively. The four batteries underwent a cycle aging test at room temperature (24 ℃), with each cycle consisting of charging and discharging modes. The charging

mode is further divided into two charging phases. In the first charging phase, the battery was charged at a 1.5 A constant current until its voltage reached 4.2 V. Then, the voltage was maintained at 4.2 V in the second charging phase until the current was reduced to 20 mA. For the discharging mode, the battery was discharged at a 2 A constant current until the voltage dropped to a certain cutoff threshold, which indicates that a complete charging-discharging cycle was completed. The life-long capacity degradation trajectories of the four batteries are shown in Fig. 4.

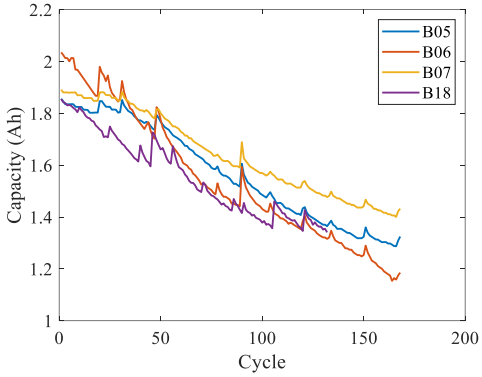

Fig. 4. Four capacity decay curves of the NASA battery dataset.

Existing literature has demonstrated that when the capacity degrades to 70-80% of its rated capacity, the performance of these aged batteries can exhibit significantly different characteristics under the same normal operation. In this paper, 1.4 Ah (70% of rated capacity) is considered as the failure threshold. However, from Fig. 4, it can be observed that the battery B0007 did not reach the failure threshold before the end of the test. Therefore, we select 1.45 Ah (72.5% of rated capacity) as the failure threshold of B0007 to carry out the subsequent analysis.

Additionally, to ensure the reconstructed capacity matrix with an equal scale in each sub-space, we employed the *mapminmax* function to normalize them individually. This not only balanced the capacity prediction weight but also effectively reduced the prediction difference among different sub-spaces.

$$X' = \frac{X - X_{\min}}{X_{\max} - X_{\min}} \tag{19}$$

where X and X' represent the raw data and the corresponding normalized data, respectively, while $X_{\max}$ and $X_{\min}$ denote the maximum and minimum values, respectively.

B. Evaluation Criteria

To assess the RUL prediction performance of the proposed hybrid model, the mean absolute error (MAE), root mean square error (RMSE), R-squared error (R^2), and absolute error are adopted as evaluation metrics. They are defined as follows:

$$MAE = \frac{1}{N}\sum_{i=1}^{N}\left|\hat{Q}_i - Q_i\right| \tag{20}$$

$$RMSE = \sqrt{\frac{1}{N}\sum_{i=1}^{N}(\hat{Q}_i - Q_i)^2} \tag{21}$$

$$R^2 = 1 - \frac{\sum_{i=1}^{N}(\hat{Q}_i - Q_i)^2}{\sum_{i=1}^{N}(Q_i - \bar{Q}_i)^2} \tag{22}$$

$$AE = \left|RUL_p - RUL_r\right| \tag{23}$$

where $\hat{Q}_i$ is the predicted capacity value, Q_i represents actual capacity value, $\bar{Q}_i$ is the average value of actual capacity Q_i, RUL_p and RUL_r denote the predicted and real RUL values, respectively. For *MAE*, *RMSE*, and *AE*, higher RUL prediction accuracy is achieved when their values are closer to zero. In contrast, the R^2 value closer to one indicates a better fit of the model.

C. Analysis and Discussion of Results

We can obtain the delays of B0005, B0006, B0007, and B018 are 1, 2, 2, and 4, respectively, according to (2) - (4). To evaluate the prediction performance of the hybrid CNN-BiLSTM-HAM model, we compare its accuracy and stability against four other different models: LSTM, BiLSTM, CNN-BiLSTM, and CNN-BiLSTM-SHA. Furthermore, the generalization ability of the hybrid model is demonstrated by using three different starting points for the training and testing sets: the 30th, 50th, and 70th cycles.

In these experiments, all models were trained with the first 30, 50, and 70 cycles of known capacity data from the NASA battery dataset. The prediction results of the five models are depicted in Figs. 5-8, respectively. Correspondingly, Tables II-V display the comparative results of RUL_{p}, AE, MAE, RMSE, and R^2 for all models under different prediction starting points, respectively. From Figs. 5-8, we can clearly observe that the capacity prediction trajectories of the proposed hybrid model, CNN-BiLSTM-HAM, align more closely with the actual capacity degradation trajectory for the same prediction starting point compared to the results of the other four models.

Tables II-V also clearly show that the prediction errors, MAE, and RMSE of the proposed method are lower than those of the other four methods for RUL prediction. In addition, the proposed method demonstrates the closest RUL_{p} to RUL_{r}, the smallest AE, and the highest R^2 value. These results strongly validate the excellent performance and robustness of our proposed hybrid model in addressing the battery RUL prediction problem.

Taking the starting point of the 50th cycle of the B0005 battery as an example, the MAE and RMSE of the predicted results are reduced by 24.61% to 76.94% and 22.09% to 71.05%, respectively. Compared to CNN-BiLSTM-SHA, the proposed CNN-BiLSTM-HAM achieves an attention score matrix across different sub-spaces, which improves the model's ability to capture data nonlinearity and complexity. Furthermore, the prediction errors of CNN-BiLSTM are higher than those of CNN-BiLSTM-SHA, highlighting SHA's capability to enhance key information characterization through learnable weights, thereby improving prediction accuracy. To illustrate this more intuitively, the AE results show that the starting point 50th cycle of B0005 battery RUL_{r} is the 74 cycle,

This article has been accepted for publication in IEEE Journal of Emerging and Selected Topics in Industrial Electronics. This is the author's version which has not been fully edited and content may change prior to final publication. Citation information: DOI 10.1109/JESTIE.2025.3561664

and the predicted RUL is 75 from the proposed model with an error of only one cycle. In contrast, the RUL predictions of the other four models are 71, 68, 81, and 86, respectively, and the respective errors are 3, 6, 7, and 12 cycles.

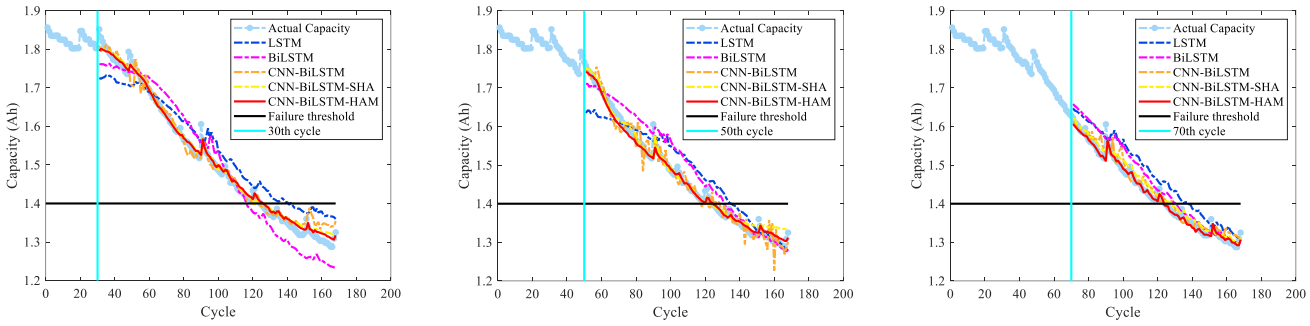

(a) B0005-30th cycle (b) B0005-50th cycle (c) B0005-70th cycle

Fig. 5. B0005 battery capacity prediction with different amounts of training data.

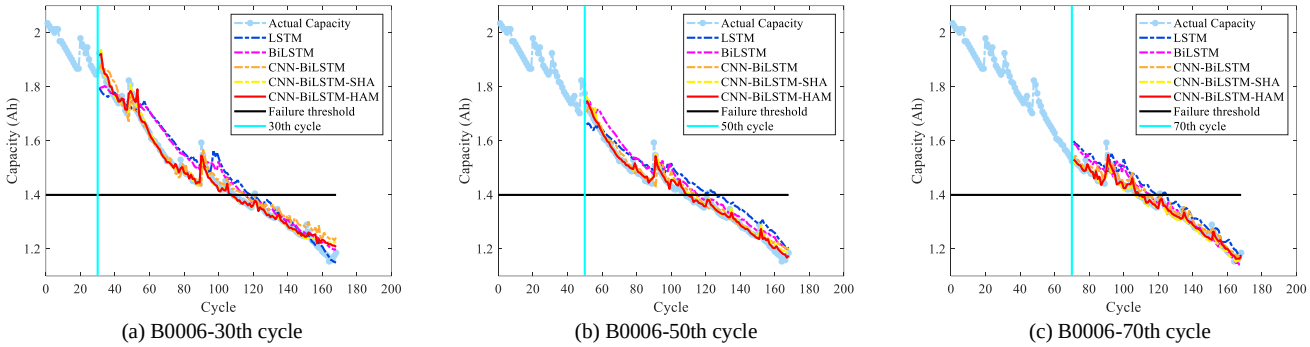

(a) B0006-30th cycle (b) B0006-50th cycle (c) B0006-70th cycle

Fig. 6. B0006 battery capacity prediction with different amounts of training data.

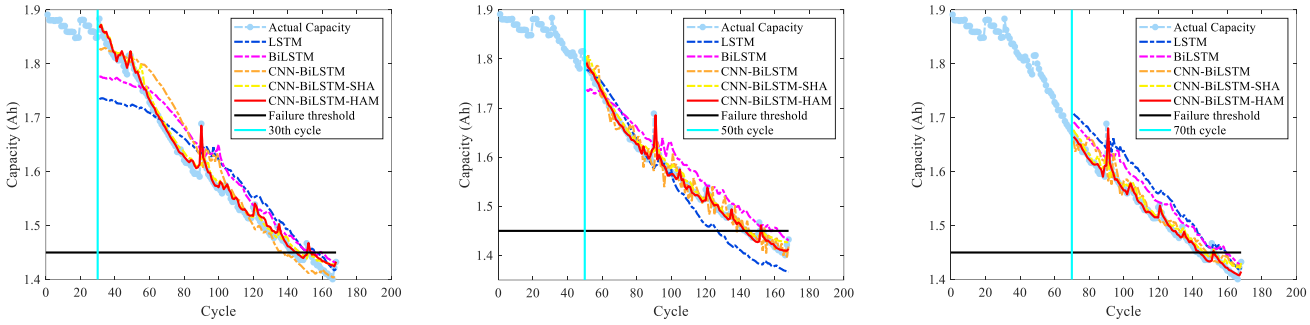

(a) B0007-30th cycle (b) B0007-50th cycle (c) B0007-70th cycle

Fig. 7. B0007 battery capacity prediction with different amounts of training data.

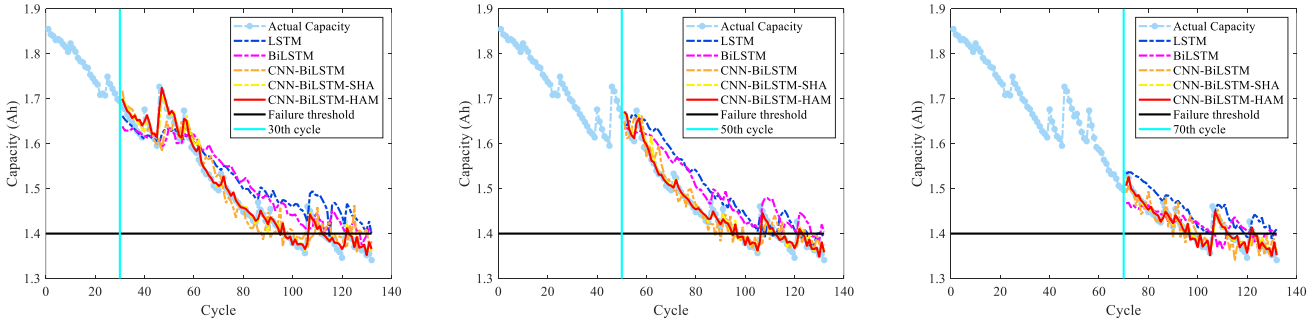

(a) B0018-30th cycle (b) B0018-50th cycle (c) B0018-70th cycle

Fig. 8. B0018 battery capacity prediction with different amounts of training data.

TABLE II
COMPARISON OF RUL PREDICTION RESULTS OF B0005

Models	Cycle	RUL_r	RUL_p	AE	MAE	RMSE	R^2
PSR-LSTM [20]			111	17	0.0471	0.0517	0.8517
PSR-BiLSTM [22]			87	7	0.0397	0.0450	0.8755
PSR-CNN-BiLSTM [22]	30	94	90	6	0.0181	0.0243	0.9283
PSR-CNN-BiLSTM-SHA [23]			91	3	0.0124	0.0159	0.9607
PSR-CNN-BiLSTM-HMA			**96**	**2**	**0.0101**	**0.0142**	**0.9725**
PSR-LSTM [20]			86	12	0.0412	0.0487	0.8667
PSR-BiLSTM [22]			81	7	0.0345	0.0416	0.9024
PSR-CNN-BiLSTM [22]	50	74	68	6	0.0186	0.0241	0.9672
PSR-CNN-BiLSTM-SHA [23]			71	3	0.0126	0.0181	0.9813
PSR-CNN-BiLSTM-HMA			**75**	**1**	**0.0095**	**0.0141**	**0.9889**
PSR-LSTM [20]			68	14	0.0445	0.0477	0.7621
PSR-BiLSTM [22]			61	7	0.0311	0.0361	0.8632
PSR-CNN-BiLSTM [22]	70	54	59	5	0.0173	0.0216	0.9512
PSR-CNN-BiLSTM-SHA [23]			58	4	0.0139	0.0168	0.9703
PSR-CNN-BiLSTM-HMA			**54**	**0**	**0.0068**	**0.0129**	**0.9923**

Note: Marked with red and bold are the best evaluation metric values.

TABLE III
COMPARISON OF RUL PREDICTION RESULTS OF B0006

Models	Cycle	RUL_r	RUL_p	AE	MAE	RMSE	R^2
PSR-LSTM [20]			89	10	0.0451	0.0561	0.8626
PSR-BiLSTM [22]			86	7	0.0403	0.0486	0.8844
PSR-CNN-BiLSTM [22]	30	79	86	7	0.0272	0.0368	0.9123
PSR-CNN-BiLSTM-SHA [23]			77	2	0.0137	0.0227	0.9656
PSR-CNN-BiLSTM-HMA			**78**	**1**	**0.0128**	**0.0194**	**0.9796**
PSR-LSTM [20]			76	17	0.0485	0.0521	0.8667
PSR-BiLSTM [22]			66	7	0.0388	0.0434	0.9067
PSR-CNN-BiLSTM [22]	50	59	65	6	0.0213	0.0291	0.9586
PSR-CNN-BiLSTM-SHA [23]			62	3	0.0135	0.0199	0.9803
PSR-CNN-BiLSTM-HMA			**60**	**1**	**0.0095**	**0.0169**	**0.9858**
PSR-LSTM [20]			49	10	0.0441	0.0486	0.7964
PSR-BiLSTM [22]			46	7	0.0279	0.0357	0.8901
PSR-CNN-BiLSTM [22]	70	39	43	4	0.0191	0.0233	0.9529
PSR-CNN-BiLSTM-SHA [23]			37	2	0.0116	0.0182	0.9715
PSR-CNN-BiLSTM-HMA			**39**	**0**	**0.0085**	**0.0158**	**0.9883**

Note: Marked with red and bold are the best evaluation metric values.

TABLE IV
COMPARISON OF RUL PREDICTION RESULTS OF B0007

Models	Cycle	RUL_r	RUL_p	AE	MAE	RMSE	R^2
PSR-LSTM [20]			126	12	0.0414	0.0493	0.8659
PSR-BiLSTM [22]			125	11	0.0356	0.0406	0.9091
PSR-CNN-BiLSTM [22]	30	113	108	5	0.0292	0.0371	0.9239
PSR-CNN-BiLSTM-SHA [23]			117	4	0.0114	0.0141	0.9789
PSR-CNN-BiLSTM-HMA			**115**	**2**	**0.0082**	**0.0115**	**0.9841**
PSR-LSTM [20]			77	16	0.0335	0.0394	0.8581
PSR-BiLSTM [22]			108	15	0.0303	0.0331	0.8989
PSR-CNN-BiLSTM [22]	50	93	88	5	0.0154	0.0211	0.9593
PSR-CNN-BiLSTM-SHA [23]			95	2	0.0102	0.0134	0.9835
PSR-CNN-BiLSTM-HMA			**93**	**0**	**0.0064**	**0.0106**	**0.9907**

PSR-LSTM [20]			89	16	0.0429	0.0456	0.6405
PSR-BiLSTM [22]			87	14	0.0314	0.0334	0.8074
PSR-CNN-BiLSTM [22]	70	73	79	6	0.0174	0.0211	0.9125
PSR-CNN-BiLSTM-SHA [23]			77	4	0.0099	0.0128	0.9716
PSR-CNN-BiLSTM-HMA			**74**	**1**	**0.0055**	**0.0102**	**0.9967**

Note: Marked with red and bold are the best evaluation metric values.

TABLE V
COMPARISON OF RUL PREDICTION RESULTS OF B0018

Models	Cycle	RUL_r	RUL_p	AE	MAE	RMSE	R^2
PSR-LSTM [20]			85	18	0.0473	0.0547	0.7566
PSR-BiLSTM [22]			83	16	0.0427	0.0493	0.8028
PSR-CNN-BiLSTM [22]	30	67	57	10	0.0302	0.0378	0.8838
PSR-CNN-BiLSTM-SHA [23]			60	7	0.0121	0.0191	0.9708
PSR-CNN-BiLSTM-HMA			**65**	**2**	**0.0102**	**0.0157**	**0.9898**
PSR-LSTM [20]			65	18	0.0501	0.0565	0.5585
PSR-BiLSTM [22]			58	11	0.0463	0.0493	0.6651
PSR-CNN-BiLSTM [22]	50	47	38	9	0.0218	0.0274	0.8963
PSR-CNN-BiLSTM-SHA [23]			44	3	0.0109	0.0159	0.9648
PSR-CNN-BiLSTM-HMA			**45**	**2**	**0.0086**	**0.0142**	**0.9919**
PSR-LSTM [20]			36	9	0.0408	0.0431	0.7911
PSR-BiLSTM [22]			35	8	0.0299	0.0351	0.5891
PSR-CNN-BiLSTM [22]	70	27	20	7	0.0192	0.0242	0.8094
PSR-CNN-BiLSTM-SHA [23]			28	1	0.0085	0.0156	0.8791
PSR-CNN-BiLSTM-HMA			**27**	**0**	**0.0077**	**0.0134**	**0.9876**

Note: Marked with red and bold are the best evaluation metric values.

To demonstrate the superiority of the PSR with the C-C method, we compare the embedding spatial-temporal capacity matrix by PSR with the original one-dimensional data as the inputs for the CNN-BLSTM-HAM model. The prediction errors are shown in Table VI. We conclude from Table VI that the PSR-based capacity matrix with the C-C method yields better prediction results than the original one-dimensional capacity data. This improvement is due to the fact that the embedding spatial-temporal capacity matrix contributes to better capability in capturing the underlying nonlinear relationships and dynamic characteristics, which improves the accuracy of feature extraction, analysis, and modeling.

TABLE VI
COMPARISON OF PHASE SPACE RECONSTRUCTION

Battery	Cycle	Method	RMSE	R^2
B0005	30	CNN-BiLSTM-HMA	0.0151	0.9615
		PSR-CNN-BiLSTM-HMA	**0.0142**	**0.9725**
	50	CNN-BiLSTM- HMA	0.0138	0.9846
		PSR-CNN-BiLSTM-HMA	**0.0141**	**0.9889**
	70	CNN-BiLSTM- HMA	0.0139	0.9795
		PSR-CNN-BiLSTM-HMA	**0.0129**	**0.9923**
B0006	30	CNN-BiLSTM-HMA	0.0212	0.9675
		PSR-CNN-BiLSTM-HMA	**0.0194**	**0.9796**
	50	CNN-BiLSTM- HMA	0.0192	0.9818
		PSR-CNN-BiLSTM-HMA	**0.0169**	**0.9858**
B0007	70	CNN-BiLSTM- HMA	0.0173	0.9741
		PSR-CNN-BiLSTM-HMA	**0.0158**	**0.9883**
	30	CNN-BiLSTM-HMA	0.0146	0.9782
		PSR-CNN-BiLSTM-HMA	**0.0115**	**0.9841**
	50	CNN-BiLSTM- HMA	0.0124	0.9860
		PSR-CNN-BiLSTM-HMA	**0.0106**	**0.9907**
	70	CNN-BiLSTM- HMA	0.0115	0.9771
		PSR-CNN-BiLSTM-HMA	**0.0102**	**0.9967**
B0018	30	CNN-BiLSTM-HMA	0.0192	0.9702
		PSR-CNN-BiLSTM-HMA	**0.0157**	**0.9898**
	50	CNN-BiLSTM- HMA	0.1702	0.9601
		PSR-CNN-BiLSTM-HMA	**0.0142**	**0.9919**
	70	CNN-BiLSTM- HMA	0.0177	0.8441
		PSR-CNN-BiLSTM-HMA	**0.0134**	**0.9876**

Note: Marked with red and bold are the best evaluation metric values.

To further demonstrate the superiority of the proposed method, a comparison with several advanced RUL prediction techniques is presented in Table VII. Considering the extensive research achievements in RUL prediction based on battery B0005, this battery is selected in Table VII to facilitate a clear comparison with the existing studies in the literature. Although our method imposes a higher computational burden, the MAE and RMSE error metrics clearly show that the proposed method outperforms several

previously published RUL prediction techniques. In practical applications, especially in energy storage systems, large battery packs are often assembled. Due to the complexity and non-direct observability of the internal aging mechanisms, accurately predicting the RUL of all batteries is challenging. Consequently, data-driven methods relying on degradation capacity data and hybrid models offer an effective solution. In this sense, balancing accuracy and computational efficiency is both practical and essential, which provides significant potential for future applications in battery pack RUL prediction techniques.

TABLE VII
PERFORMANCE COMPARISON OF DIFFERENT METHODS FOR BATTERY B0005

Method	Cycle	AE	RMSE	Time(s)
SVM [19]		16	0.1134	**1.28**
GWO-SVM [21]		14	0.1021	6.13
LSTM-SVM [21]		5	0.0583	4.48
UKF [28]	30	19	0.1389	2.56
AUKF [28]		10	0.0832	3.25
AUKF-SVM [28]		8	0.0756	3.98
Proposed		**2**	**0.0142**	5.79
SVM [19]		11	0.0696	**1.37**
GWO-SVM [21]		11	0.0622	7.72
LSTM-SVM [21]		4	0.0287	4.78
UKF [28]	50	14	0.0944	2.98
AUKF [28]		7	0.0513	3.66
AUKF-SVM [28]		5	0.0453	4.23
Proposed		**1**	**0.0141**	5.94
SVM [19]		8	0.0537	**1.54**
GWO-SVM [21]		8	0.0482	11.41
LSTM-SVM [21]		1	0.0168	5.13
UKF [28]	70	11	0.0817	3.64
AUKF [28]		6	0.0344	4.37
AUKF-SVM [28]		3	0.0239	4.86
Proposed		**0**	**0.0129**	6.27

Note: Marked with red and bold are the best evaluation metric values.

IV. CONCLUSION AND FUTURE WORK

In order to overcome the poor stability of single models and the redundancy and insufficiency of data in conventional data-driven approaches, this paper proposes a degradation capacity spatial-temporal embedding RUL prediction framework and a CNN-BiLSTM-HAM hybrid model. Specifically, the time delay and embedding dimension are calculated by the C-C method with two correlated integrals, allowing for the argumentation and reconstruction of capacity data. This process helps the network uncover more valuable information. In this hybrid model, the CNN is employed to extract rich feature maps from the reconstructed matrix, which are then fed into a BiLSTM network comprised of two independently and inversely processed LSTM units. Finally, the HAM method is introduced to selectively and dynamically adjust corresponding weights of various degradation rate stages that can be effectively captured and updated to improve RUL prediction precision. Although satisfactory results are achieved in this study, several aspects are worth further exploration:

1) Interpretability of neural networks: The inherent "black box" nature of neural networks limits the transparency of the prediction process. Future research should focus on enhancing the interpretability and trustworthiness of the model by introducing interpretable artificial intelligence methods, such as analyzing the significance of aging features.

2) Extension to battery packs: In practical applications, such as energy storage systems, multiple batteries are typically assembled into a battery pack. Extending RUL prediction to the entire battery pack is essential, considering the interactions among individual batteries and the impact of energy management strategies within the pack.

REFERENCES

[1] Y. Che, X. Hu, X. Lin, et al., "Health prognostics for lithium-ion batteries: mechanisms, methods, and prospects," *Energy Environ. Sci.*, vol. 16, no. 2, pp. 338-371, Jan. 2023, doi: 10.1039/D2EE03019E.

[2] K. Zhang, Z. Peng, C. Sun, et al., "Remaining useful life prediction of aircraft lithium-ion batteries based on F-distribution particle filter and kernel smoothing algorithm," *Chin. J. Aeronaut.*, vol. 33, no. 5, pp. 1517-1531, May. 2020, doi: 10.1016/j.cja.2020.01.007.

[3] Y. Zhao, Z. Wang, Z. Sun, et al., "Data-driven lithium-ion battery degradation evaluation under overcharge cycling conditions," *IEEE Trans. Power Electron.*, vol. 38, no. 8, pp. 10138-10150, Aug. 2023, doi: 10.1109/TPEL.2023.3280576.

[4] Y. Li, M. Vilathgamuwa, B. Xiong, et al., "Design of minimum cost degradation-conscious lithium-ion battery energy storage system to achieve renewable power dispatchability," *Appl. Energy.*, vol. 260, pp. 114282, Feb. 2020, doi:10.1016/j.apenergy.2019.114282.

[5] R. Xiong, W. Sun, Q. Yu, et al., "Research progress, challenges and prospects of fault diagnosis on battery system of electric vehicles," *Appl. Energy.*, vol. 279, no. 115855, Dec. 2020, doi: 10.1016/j.apenergy.2020.115855.

[6] S. Wen, Y. Wang, Y. Tang, Y. Xu, P. Li, and T. Zhao, "Real-time identification of power fluctuations based on LSTM recurrent neural network: A case study on Singapore power system," *IEEE Trans. Ind. Informat.*, vol. 15, no. 9, pp. 5266-5275, Sept. 2019, doi: 10.1109/TII.2019.2910416.

[7] X. Cong, C. Zhang, J. Jiang, et al., "A hybrid method for the prediction of the remaining useful life of lithium-ion batteries with accelerated capacity degradation," *IEEE Trans. Veh. Technol.*, vol. 69, no. 11, pp. 12775-12785, Sep. 2020, doi: 10.1109/TVT.2020.3024019.

[8] C. Lin, J. Xu, X. Mei, "Improving state-of-health estimation for lithium-ion batteries via unlabeled charging data," *Energy Storage Mat.*, vol. 54, pp. 85-97, Jan. 2023, doi: 10.1016/j.ensm.2022.10.030.

[9] R. Xiong, Y. Sun, C. Wang, et al., "A data-driven method for extracting aging features to accurately predict the battery health," *Energy Storage Mat.*, vol. 57, pp. 460-470, Mar. 2023, doi: 10.1016/j.ensm.2023.02.034.

[10] S. Hong, C. Qin, X. Lai, et al., "State-of-health estimation and remaining useful life prediction for lithium-ion batteries based on an improved particle filter algorithm," *J. Energy Storage*, vol. 64, pp. 107179, Aug. 2023, doi: 10.1016/j.est.2023.107179.

[11] J. Wu, Z. Wei, W. Li, Y. Wang, Y. Li, and D. U. Sauer, "Battery thermal- and health-constrained energy management for hybrid electric bus based on soft actor-critic DRL algorithm," *IEEE Trans. Ind. Informat.*, vol. 17, no. 6, pp. 3751-3761, June 2021, doi: 10.1109/TII.2020.3014599.

[12] B. Li, K. Xie, W. Zhong, et al., "Operation management of electric vehicle battery swapping and charging systems: A bilevel optimization approach," *IEEE Trans. Intell. Transp. Syst.*, vol. 24, no. 1, pp. 528-540, Jan. 2023, doi: 10.1109/TITS.2022.3211883.

[13] G. Huber, K. Bogenberger, and H. van Lint, "Optimization of charging strategies for battery electric vehicles under uncertainty," *IEEE Trans. Intell. Transp. Syst.*, vol. 23, no. 2, pp. 760-776, Feb. 2022, doi: 10.1109/TITS.2020.3027625.

[14] D. Li, Z. Zhang, P. Liu, et al., "Battery fault diagnosis for electric vehicles based on voltage abnormality by combining the long short-term memory neural network and the equivalent circuit model," *IEEE Trans. Power Electron.*, vol. 36, no. 2, pp. 1303-1315, Feb. 2021, doi: 10.1109/TPEL.2020.3008194.

[15] L. Ren, J. Dong, X. Wang, et al., "A data-driven auto-CNN-LSTM prediction model for lithium-ion battery remaining useful life," *IEEE Trans. Ind. Informat.*, vol. 17, no. 5, pp. 3478-3487, May 2021, doi: 10.1109/TII.2020.3008223.

[16] X. Shu, J. Shen, G. Li, et al., "A flexible state-of-health prediction scheme for lithium-ion battery packs with long short-term memory network and transfer learning," *IEEE Trans. Transport. Electrific.*, vol. 7, no. 4, pp. 2238-2248, Dec. 2021, doi: 10.1109/TTE.2021.3074638.

[17] Y. Wang, C. Zhou, and Z. Chen, "An enhanced approach for load behavior and battery residual capacity prediction using Markov chain and Monte Carlo method," *IEEE J. Emerg. Sel. Topics Ind. Electron.*, vol. 4, no. 1, pp. 159-167, Jan. 2023, doi: 10.1109/JESTIE.2021.3115468.

[18] S. Saxena, L. Ward, J. Kubal, et al., "A convolutional neural network model for battery capacity fade curve prediction using early life data," *J. Power Sources.*, vol. 542, pp. 231736, Sep. 2022, doi: 10.1016/j.jpowsour.2022.231736.

[19] D. Swain, M. Kumar, A. Nour, et al., "Remaining useful life predictor for EV batteries using machine learning," *IEEE Access.*, vol. 12, pp. 134418-134426, Sep.2024, doi: 10.1109/ACCESS.2024.3461802.

[20] B. Zraibi, C. Okar, H. Chaoui, and M. Mansouri, "Remaining useful life assessment for lithium-ion batteries using CNN-LSTM-DNN hybrid method," *IEEE Trans. Veh. Technol.*, vol. 70, no. 5, pp. 4252-4261, May 2021, doi: 10.1109/TVT.2021.3071622.

[21] Z. Lyu, G. Wang, and R. Gao, "Li-ion battery prognostic and health management through an indirect hybrid mode," *J. Energy Storage.*, vol. 42, pp. 102990, Oct. 2021, doi: 10.1016/j.est.2021.102990.

[22] R. Ardeshiri, M. Liu, and C. Ma, "Multivariate stacked bidirectional long short term memory for lithium-ion battery health management," *Rel. Eng. Syst. Saf.*, vol. 224, pp. 108481, Aug. 2022, doi: 10.1016/j.ress.2022.108481.

[23] J. Zhang, X. Li, J. Tian, et al., "An integrated multi-head dual sparse self-attention network for remaining useful life prediction," *Rel. Eng. Syst. Saf.*, vol. 233, pp. 109096, May 2023, doi: 10.1016/j.ress.2023.109096.

[24] F. Takens, "Detecting strange attractors in turbulence," *Dynamical Systems and Turbulence, Warwick 1980: proceedings of a symposium held at the University of Warwick 1979/80. Berlin, Heidelberg: Springer Berlin Heidelberg*, pp. 366-381, 2006.

[25] H. S. Kim, R. Eykholt, and J. D. Salas, "Nonlinear dynamics, delay times, and embedding windows," *Physica D: Nonlinear Phenomena.*, vol. 127, no. 1-2, pp. 48-60, Mar 1999, doi: 10.1016/S0167-2789(98)00240-1.

[26] L. Su, "Prediction of multivariate chaotic time series with local polynomial fitting," *Comput. Math. Appl.*, vol. 59, no. 2, pp. 737-744, Jan 2010, doi: 10.1016/j.camwa.2009.10.019.

[27] C. Liu, Y. Wang, and Z. Chen, "Degradation model and cycle life prediction for lithium-ion battery used in hybrid energy storage system," *Energy.*, vol. 166, pp. 796-806, Jan 2019, doi: 10.1016/j.energy.2018.10.131.

[28] Z. Xue, Y. Zhang, C. Cheng, et al., "Remaining useful life prediction of lithium-ion batteries with adaptive unscented kalman filter and optimized support vector regression," *Neurocomput.*, vol. 376, pp. 95-102, Sep. 2020, doi: 10.1016/j.neucom.2019.09.074.

Laijin Luo received the M.S. degree in information and communication Engineering from Anqing Normal University, Anhui, China, in 2024. He is currently pursuing the Ph.D. degree with the School of Electrical Engineering, Chongqing University, Chongqing, China. His research interests include battery modeling, state estimation and deep learning.

Yu Wang (S'12-M'17-SM'23) received B.Eng. degree in Electrical Engineering and Automation from Wuhan University, China in 2011, M.Sc. and Ph.D. degree in Power Engineering from Nanyang Technological University (NTU), Singapore in 2012 and 2017, respectively. Currently, he is a professor at the School of Electrical Engineering, Chongqing University, China. He was a Marie Skłodowska-Curie Individual Fellow at Control and Power Group, Imperial College London. He serves as the Associated Editor of *Journal of Modern Power Systems and Clean Energy*, *IET Generation, Transmission and Distribution*, and *IET Renewable Power Generation*. His research interests include microgrid operation and control, power system dynamics and control, and cyber-physical power systems.

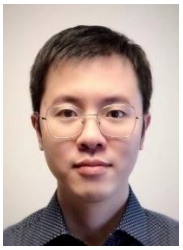

Yang Li (Senior Member) received the B.E. degree in electrical engineering from Wuhan University, Wuhan, China, in 2007, and the M.Sc. and Ph.D. degrees in power engineering from Nanyang Technological University (NTU), Singapore, in 2008 and 2015, respectively. He was with the Energy Research Institute, NTU and the School of Electrical Engineering and Computer Science, Queensland University of Technology, Brisbane, QLD, Australia, and the School of Automation, Wuhan University of Technology, Wuhan, from 2016 to 2020. Since 2020, he has been a Researcher with the Department of Electrical Engineering, Chalmers University of Technology, Gothenburg, Sweden. His research interests include modeling and control of energy storage systems in power and transport sectors. Dr. Li serves as an Associate Editor for several journals such as IEEE TRANSACTIONS ON TRANSPORTATION ELECTRIFICATION, IEEE TRANSACTIONS ON INDUSTRIAL ELECTRONICS, and IEEE TRANSACTIONS ON ENERGY CONVERSION, and was a Guest Editorial Member for IEEE TRANSACTIONS ON INDUSTRIAL APPLICATIONS, *IET Renewable Power Generation*, and *Applied Energy*.

Qiushi Cui (Member, IEEE) earned his M.Sc. degree from Illinois Institute of Technology, and the Ph.D. degree from McGill University, both in Electric Engineering. Currently, he is an associate professor from School of Electrical Engineering at Chongqing University. He was working as a postdoctoral researcher at of Arizona State University (ASU) and served as the Associate Director of Machine Learning Laboratory for Power Systems in the Ira A. Fulton Schools of Engineering of the same university. Prior to joining ASU, he was a Research Engineer at OPAL-RT Technologies Inc. from Nov. 2015 to Nov. 2017. His research interests are in the areas of machine learning and big data applications in power systems, power system protection, smart cities, microgrid, EV integration, and realtime simulation in power engineering. Dr. Cui has won three Best Paper Awards from UK, China, and the USA, all ranking the first. He was the winner of the Chunhui Cup Innovation and Entrepreneurship Competition for Overseas Chinese Scholars in the Energy Sector in 2018. Dr. Cui received the Postdoctoral Research Scholarship from both Natural Sciences and Engineering Research Council of Canada (NSERC) and Quebec Research Fund-Nature and Technology (FRQNT) and held the MITACS Accelerate Research Program Fellowship from Canada.